applied sciences

MDPI

Article

Advanced Nested Coaxial Thin-Film ZnO Nanostructures Synthesized by Atomic Layer Deposition for Improved Sensing Performance

Pengtao Lin [1,2], Lari S. Zhang [2], Kai Zhang [1,2] and Helmut Baumgart [1,2,*]

[1] Department of Electrical and Computer Engineering, Old Dominion University, Norfolk, VA 23529, USA; linpt1016@gmail.com (P.L.); kkaizhang@gmail.com (K.Z.)
[2] ODU-Applied Research Center at Thomas Jefferson National Accelerator Laboratories, 12050 Jefferson Avenue, Suite 721, Newport News, VA 23606, USA; larizhang531@gmail.com
* Correspondence: hbaumgar@odu.edu

Abstract: We report a new synthesis method for multiple-walled nested thin-film nanostructures by combining hydrothermal growth methods with atomic layer deposition (ALD) thin-film technology and sacrificial films, thereby increasing the surface-to-volume ratio to improve the sensing performance of novel ZnO gas sensors. Single-crystal ZnO nanorods serve as the core of the nanostructure assembly and were synthesized hydrothermally on fine-grained ALD ZnO seed films. Subsequently, the ZnO core nanotubes were coated with alternating sacrificial coaxial 3D wrap-around ALD Al_2O_3 films and ALD ZnO films. Basically, the center nanorod was coated with an ALD 3D wrap-around Al_2O_3 sacrificial layer to realize a nested coaxial ZnO thin-film nanotube. To increase the surface-to-volume ratio of the nested multiple-film nanostructure, both the front and backside of the nested coaxial ZnO films must be exposed by selectively removing the intermittent Al_2O_3 sacrificial films. The selective removal of the sacrificial films exposes the front and backside of the free-standing ZnO films for interaction with target gases during sensing operation while steadily increasing the surface-to-volume ratio. The sensing response of the novel ZnO gas sensor architecture with nested nanotubes achieved a maximum 150% enhancement at low temperature compared to a conventional ZnO nanorod sensor.

Keywords: atomic layer deposition (ALD); synthesis of nested thin-film nanostructures; ZnO thin films; sacrificial Al_2O_3 thin films; gas sensors; nanorod/nanotube nanostructures; sensing response; sensing performance

Citation: Lin, P.; Zhang, L.S.; Zhang, K.; Baumgart, H. Advanced Nested Coaxial Thin-Film ZnO Nanostructures Synthesized by Atomic Layer Deposition for Improved Sensing Performance. *Appl. Sci.* **2024**, *14*, 10959. https://doi.org/10.3390/app142310959

Academic Editors: Teodor I. Milenov, Stefan Kolev and Giorgio Biasiol

Received: 28 September 2024
Revised: 8 November 2024
Accepted: 20 November 2024
Published: 26 November 2024

1. Introduction

Zinc Oxide (ZnO) is a well-known n-type II–VI semiconducting metal oxide material widely used in solid-state gas sensor applications due to its wide band gap (3.37 eV), large excitation binding energy (~60 meV), high electrical conductivity, low synthesis cost and non-toxicity. ZnO gas sensors have been applied for the detection of toxic and harmful gases which include nitrogen oxide, hydrogen sulfide, carbon monoxide, and various volatile organic compounds [1]. The morphology of the various investigated ZnO gas sensors includes ZnO nanoparticles, one-dimensional (1D), two-dimensional (2D) and three-dimensional (3D) structures [2–5]. Among the various ZnO gas sensors, the classic ZnO nanorod structure has attracted much attention and has been widely investigated in gas detection due to its high surface-to-volume ratio, nontoxicity and ease of doping. Numerous methods have been applied to improve the sensing performance of ZnO nanorod gas sensors. For example, dopants like Pd, InSb, Ni and Ca have been introduced to enhance ZnO nanorod gas sensors for improvement of ethanol detection [6–9]. However, our present research demonstrates a significant measurable improvement of the sensing performance of ZnO nanorod gas sensors using a novel innovative nested film nanostructure design.

Herein, coaxial nested ALD thin-film nanotube structures were synthesized to improve the sensing performance of ZnO nanorods to ethanol vapor. The primary objective of the nested coaxial ZnO nanotube design is to provide two additional reaction surfaces compared to the conventional ZnO nanorod gas sensors for each added wrap-around sacrificial layer surrounding the anchoring center ZnO nanorod. Basically, the nested coaxial ZnO nanotube increases the surface-to-volume ratio further. An ALD 3D wrap-around Al_2O_3 sacrificial layer was coating each center nanorod to realize a nested coaxial nanotube consisting of free-standing ZnO thin films. The sacrificial layer was selectively removed by immersion and dissolution in a sodium hydroxide (NaOH) solution due to the different solubility ranges of Al_2O_3 and ZnO [10]. Figure 1 depicts a 3D schematic drawing of the concept of the coaxial nested tube-in-tube ZnO thin-film nanostructure device shown after selective removal of the sacrificial Al_2O_3 layer, which exposes two extra sensing surfaces separating the outer ZnO nanotube from the center ZnO nanorods. These two additional ZnO sensing surfaces fabricated by this novel process design method serve to increase the surface-to-volume ratio and to improve the sensing response of the gas sensor. Due to the average diameter size of ZnO nanorods and the available distance between nanorods synthesized by hydrothermal method, the thickness of the added sacrificial layer and the subsequent ZnO coating are restricted to approximately 20 nm. Therefore, ALD technology was applied to coat the core anchoring ZnO nanorods with 3D wrap-around Al_2O_3 sacrificial layers alternated with ALD ZnO layers with precisely controlled deposition thickness on the nanometer scale. To expose the sacrificial layer for wet etching, the precision ion polishing system (PIPS) was utilized to remove the accumulated top film covers composed of the ALD Al_2O_3 sacrificial layer and the ZnO thin films deposition.

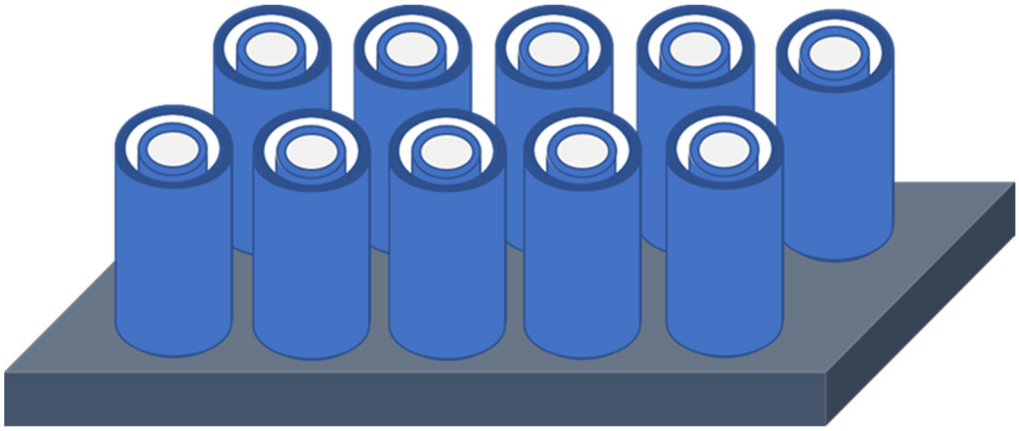

Figure 1. Schematic 3D drawing illustrating the concept of the coaxial nested tube-in-tube nanostructure design after removal of the sacrificial Al_2O_3 film separating the outer nanotube from the center nanotube, thereby exposing two new ZnO gas sensing surfaces.

For the study of the sensing performance of the novel ZnO nanotube gas sensor design to ethanol vapor concentration detection, a newly upgraded gas sensor testing system was designed and custom-built with two mass-flow controllers (MFCs) to precisely control the concentration of ethanol vapor input. We have investigated the sensing performance of the novel ZnO nanorod gas sensor design and benchmarked our nested coaxial nanotube at different temperatures with saturation-level ethanol vapor and at optimum working temperature as a function of various concentrations of ethanol vapor.

2. Materials and Methods

2.1. Sample Preparation

The following process steps were required to fabricate our novel ZnO nanorod/nanotube gas sensors. In this research, a 30 nm ZnO seed layer was deposited on p-type Si substrates by ALD system at a deposition temperature of 200 °C. The two ALD precursors for ZnO seed

layer were diethylzinc ($Zn(C_2H_5)_2$) (Sigma Aldrich, Rockville, MD, USA, CAS# 557-20-0) and deionized (DI) water, which were alternately introduced into the ALD reaction chamber by high-purity N_2 serving as a carrier gas. After ALD deposition, the ZnO samples were annealed at a temperature of 350 °C for 30 min in a thermal furnace. Subsequently, the hydrothermal solution crystal growth method was utilized for the initial ZnO nanorod growth on polycrystalline ALD ZnO seed layer, as shown in Figure 2a. The precursor solution for the ZnO nanorod hydrothermal growth was prepared with 0.03756 g zinc nitrate hexahydrate ($Zn(NO_3)6H_2O$) (Alfa Aesar, Ward Hill, MA, USA, CAS# 10196-18-6) and 0.0176 g hexamethylenetetramine ($(CH_2)_6N_4$) (Sigma Aldrich, CAS# 100-97-0) dissolved in 60 mL DI water. This ratio ensured that each chemical precursor had an exactly equal molar concentration of 20.8 mM. Afterwards, vapor phase ALD technology was employed for conformal wrap-around coating of the anchoring ZnO nanorods, first with a 20 nm Al_2O_3 sacrificial film followed by a 20 nm ZnO film using the ALD precursors trimethylamine ($Al_2(CH_3)_6$) (Sigma Aldrich, CAS# 75-24-1), diethylzinc ($Zn(C_2H_5)_2$) and DI water, as shown in Figure 2b,c. The sacrificial film serves as a "gapfiller" to separate the central hydrothermally grown anchoring ZnO nanorods from the surrounding coaxial nested nanotube film.

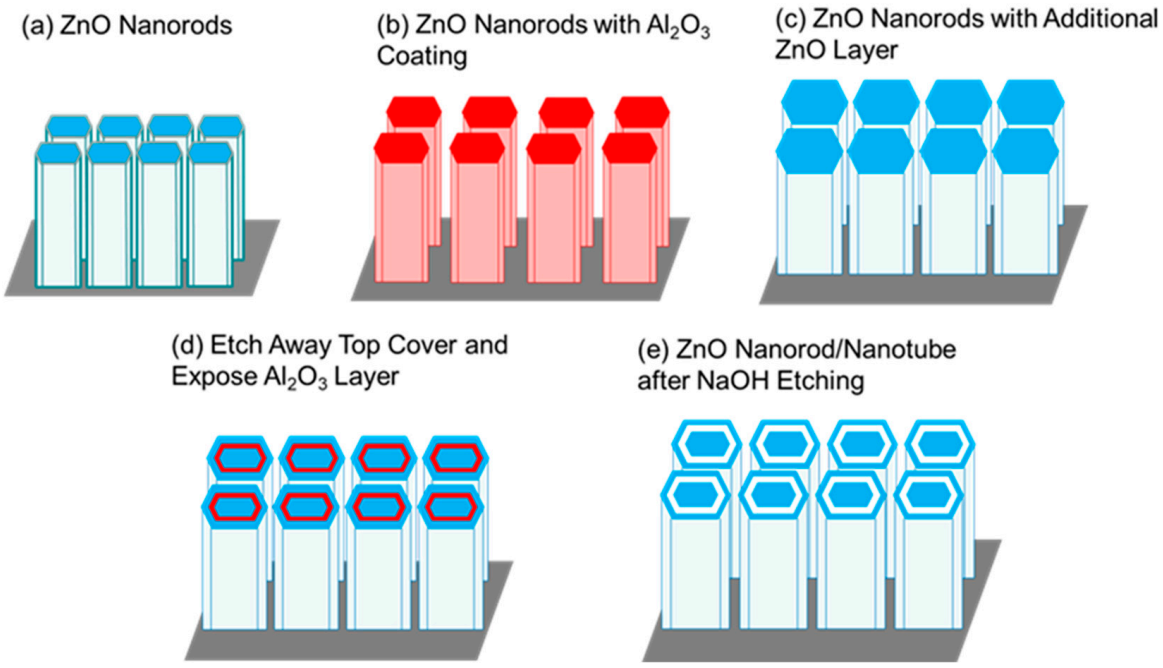

Figure 2. Schematic of process sequence fabricating coaxial nested ZnO nanorods starting with (**a**) single-crystal ZnO nanorods by hydrothermal solution growth, followed by (**b**) ZnO nanorods coated with ALD wrap-around Al_2O_3 sacrificial film, (**c**) ZnO nanorods receiving an additional coaxial wrap-around ALD ZnO film outer coating, (**d**) surface ALD film accumulation removed by PIPS and (**e**) final structure of coaxial nested wrap-around ZnO film nanostructure following the selective removal of the sacrificial film by NaOH dissolution, thereby creating the empty annular gap to expose additional sensing surfaces of the ZnO film.

Because of the surface saturating growth mechanism of ALD, all surfaces of the ZnO nanorods were completely covered with 20 nm Al_2O_3 sacrificial films, followed by another 20 nm ZnO thin film coating. To expose the Al_2O_3 sacrificial film from the top for wet chemical etch dissolution, a precision ion polishing system from Gatan Inc. was utilized to remove the surface ZnO/Al_2O_3 ALD films which conformally coated the entire outer surface of the hydrothermal ZnO nanorods, as shown in Figure 2d. After removing the accumulated ALD films only from the top surface, the sacrificial Al_2O_3 annular layer was selectively removed by immersion in an alkali sodium hydroxide solution, taking advantage of the different solubility range of Al_2O_3 and ZnO, as shown in Figure 2e. Solid

alumina can exist in solutions with pH values between 4.2 and 9.8, which means that the solubility of Al_2O_3 can be considered as below pH 4.2 and above pH 9.8 [10]. However, crystalized ZnO can only exist in a solution with a pH from 9.2 to 11.5 [10]. Therefore, an alkali solution was selected to preferentially remove the Al_2O_3 sacrificial layer without chemically attacking and damaging the center ZnO nanorods and nanotubes with pH values between 9.8 and 11.5. For this reason, in this research, a pH 11 sodium hydroxide alkali (NaOH) (Sigma Aldrich, CAS# 1310-73-2) solution was chosen for the selective wet-etch removal of the sacrificial Al_2O_3 film, creating an annular open gap and by this process exposing two additional ZnO reaction surfaces for gas sensing [10].

Figure 3 shows a cross-sectional schematic of Figure 2c–e. On the top of ZnO nanorods, several films accumulated due to conformal ALD Al_2O_3 and ZnO depositions, as shown in Figure 3a. To expose the sacrificial layer from the top, PIPS had to be used to remove the top cover with accurately controlled milling depth, shown in Figure 3b. The samples were then immersed into NaOH solution with a pH of 11 to preferentially etch off the annular sacrificial film. In this fashion, a coaxial nested ZnO nanorod/nanotube structure was created, exposing two additional reaction surfaces through the remaining open annular gap, as shown Figure 3c.

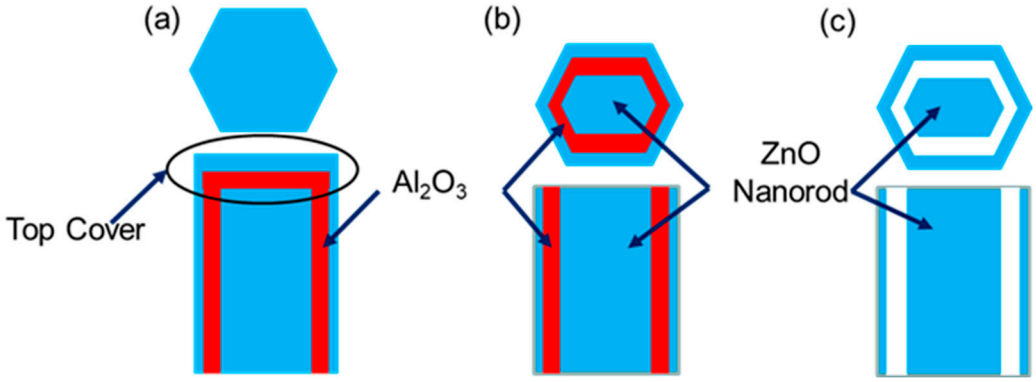

Figure 3. Cross-sectional schematic of (**a**) ZnO nanorod with ALD Al_2O_3 sacrificial film and ZnO film, (**b**) top ALD coatings removed by PIPS and (**c**) final completed nested ZnO nanotube structure after NaOH etch removal of the sacrificial alumina film exposing additional ZnO sensing surfaces.

2.2. Sensing Response Testing System

To investigate the sensing performance of our novel designed ZnO gas sensors, a gas sensor testing system was designed and custom-built by using a sealed-reaction quartz chamber and accurate temperature controller. Figure 4 shows the schematic diagram of the testing circuit built in the gas sensor testing system. The nested thin-film ZnO nanostructure gas sensor and a reference resistor were installed in a series electrical circuit. A voltage meter was used to measure the voltage changes on the reference resistor.

The sensing response of the novel ZnO gas sensor in this research is related to its DC resistance change and can be measured with an electric circuit. The resistance change is caused by redox surface reactions starting with an initial oxidation reaction between oxygen in atmospheric air and the ZnO sensing surfaces during the set operation heating up the sensor material to the optimum operating temperature. During the oxidation reaction, the majority carriers in n-type ZnO, electrons, are transferred from the conduction band to the oxidizing agent and thereby help to form one layer of negative oxygen ions on the surface of the ZnO nanotubes for the subsequent sensing reduction reaction with the target gas molecules [11]. This oxidation-induced loss of majority carriers results in a decrease of conductivity and a concomitant increase in resistivity [12]. The resistance change of the ZnO nanorod gas sensor was detected and recorded based on Equations (1)–(3), once the ZnO sample was connected to a simple electric circuit design.

$$V_{Sample} = V_{Source} - V_{Reference} \quad (1)$$

$$I = \frac{V_{Reference}}{R_{Reference}} \tag{2}$$

$$R_{Sample} = \frac{V_{Sample}}{I} = \frac{V_{Source} - V_{Reference}}{V_{Reference}/R_{Reference}} \tag{3}$$

$$Response = \frac{R_{Air} - R_{Gas}}{R_{Air}} \times 100\% \tag{4}$$

where V_{Source} is the source voltage of the testing circuit, $V_{Reference}$ is the voltage of the measurable reference resistor, I is the current of the testing circuit, R_{Sample} is the resistance of the prepared sample, R_{Air} is the resistance of the prepared sample at the testing temperature and R_{Gas} is the resistance of the prepared sample at the same testing temperature after introducing the target gas.

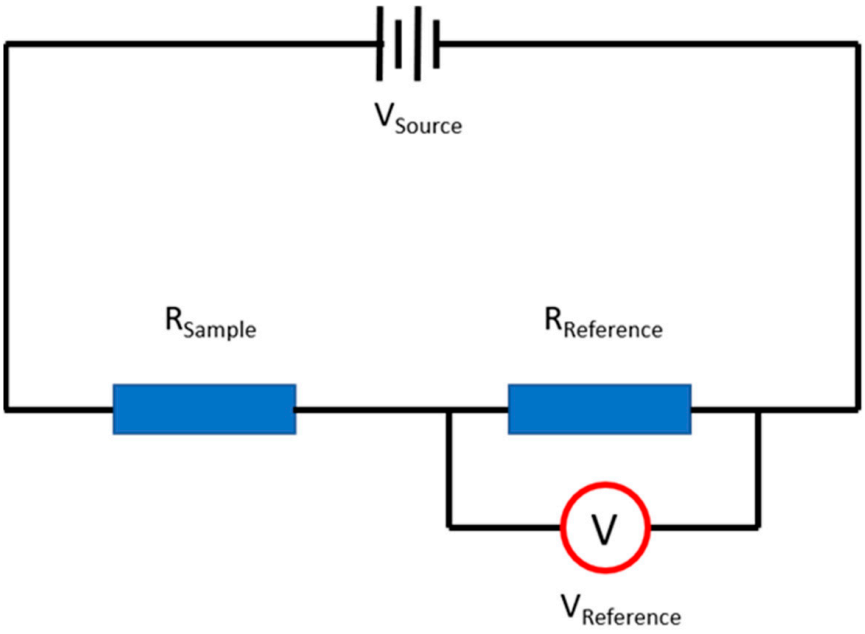

Figure 4. Schematic diagram of the testing circuit built in the gas sensor testing system.

To measure the sensing response of the ZnO nanostructures, the gas sensor testing system was developed, which included a sealed reacting chamber, a simple resistance monitoring circuit, mass flow controllers and a stable temperature controller, as shown in Figure 5.

The controller of the gas sensor testing system was based on the National Instruments Compact Rio 9068 with corresponding modules and has been programmed with LabVIEW. For the temperature control, the controller reads the real-time temperature signal from a resistance temperature detector (RTD) and provides the corresponding control signal to the heater to form a closed-loop temperature control. The controller also provides power to the electrical testing circuit and monitors the resistance change of the ZnO gas sensor [12]. To accurately control the concentration of the injected ethanol vapor in the test tube, the controller communicates with the two MFCs by providing an input volume signal and reading the real-time input volume signal, which can precisely control the concentration of the ethanol vapor on a ppm scale. Also, the humidity has been measured and was 68% during the experiments. The Dubowski equation was used to calculate the injected ethanol vapor concentration [13], as shown in Equation (5).

$$\beta_{Gas} = 0.04145 \times 10^{-3} \times \beta_{Liquid} \times \exp(0.06583 \times t) \tag{5}$$

where β_{Gas} is the mass concentration of ethanol in vapor phase in mg/L, whereas β_{Liquid} is the mass concentration of ethanol in the liquid phase in mg/L and t is the temperature in °C.

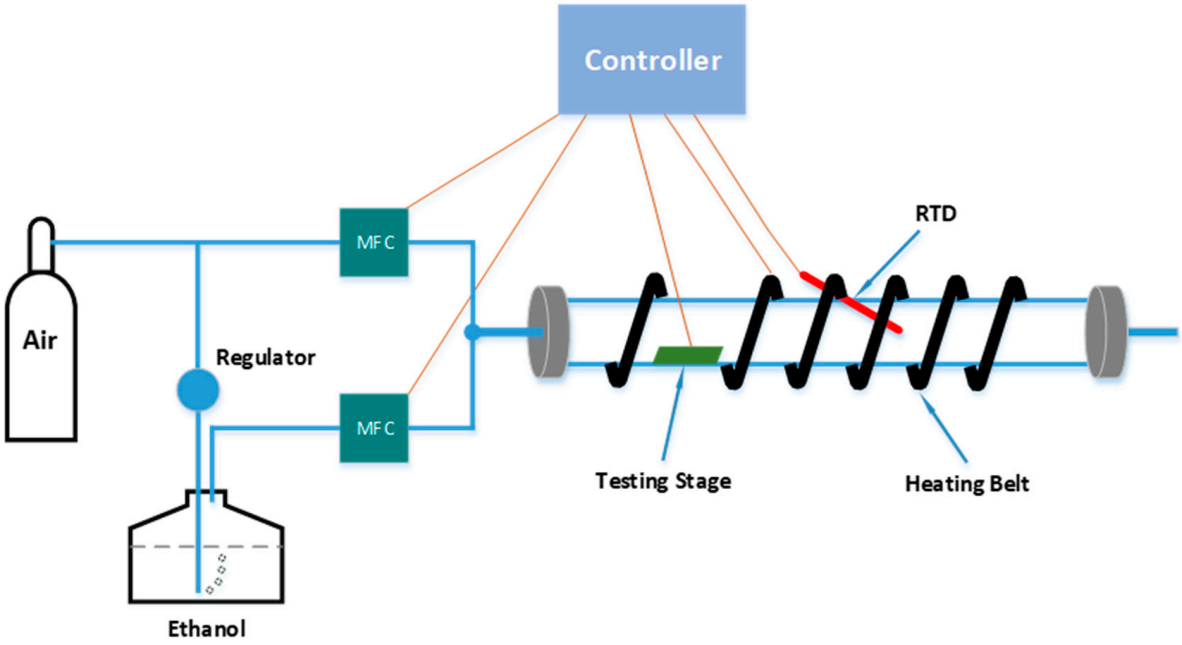

Figure 5. Schematic diagram of the improved 2nd-generation gas sensor testing system.

In this research, a Hitachi S-4700 field emission scanning electron microscope (FE-SEM) (Hitachi High-Tech Corporation, 4Pi Analysis, Inc. Durham, NC, USA) was utilized to analyze the ZnO nanorods grown from the hydrothermal methods and nested nanorod/nanotube structures after PIPS. The gas sensing performance was measured by a home-made gas sensor testing system (each data point has been tested three times, and the data showed in the image depict the average value to keep the stability of the materials).

3. Results and Discussion

3.1. Physical Characteristics of the ZnO Nanorods and Nested Nanotubes

The FE-SEM images of Figure 6a–e highlight the resulting morphology at the various stages of the entire sequence of the nested ZnO thin-film nanorod/nanotube gas sensor synthesis process. Figure 6a shows the ZnO nanorods grown by the hydrothermal method, clearly revealing single crystalline ZnO nanorods with a crystallographic hexagonal cross-section structure. Following 3D wrap-around coatings with an ALD Al_2O_3 sacrificial film and on top of it another ZnO ALD film coating, the surface of the center ZnO nanorods was covered and sealed with a top ZnO covering, as shown in Figure 6b. The PIPS process was utilized to remove the top cover and to expose the Al_2O_3 sacrificial layer from the top as shown in Figure 6c,d. Afterwards, the sacrificial alumina layer was preferentially removed by wet chemical dissolution in an NaOH alkali solution. This constitutes a key process step in our novel sensor design and isolated the center hydrothermal ZnO nanotubes. The creation of an empty annular gap remaining after the removal of the sacrificial layer exposed two additional reaction-sensing surfaces, as shown in Figure 6e. The higher magnification micrograph of Figure 6e highlights the nanotube surfaces exhibiting a granular structure which is indicative of polycrystalline material. Figure 6f shows a cross-sectional view of the ZnO nanorod/nanotube gas sensors, revealing an average nanorod height of ~750 nm.

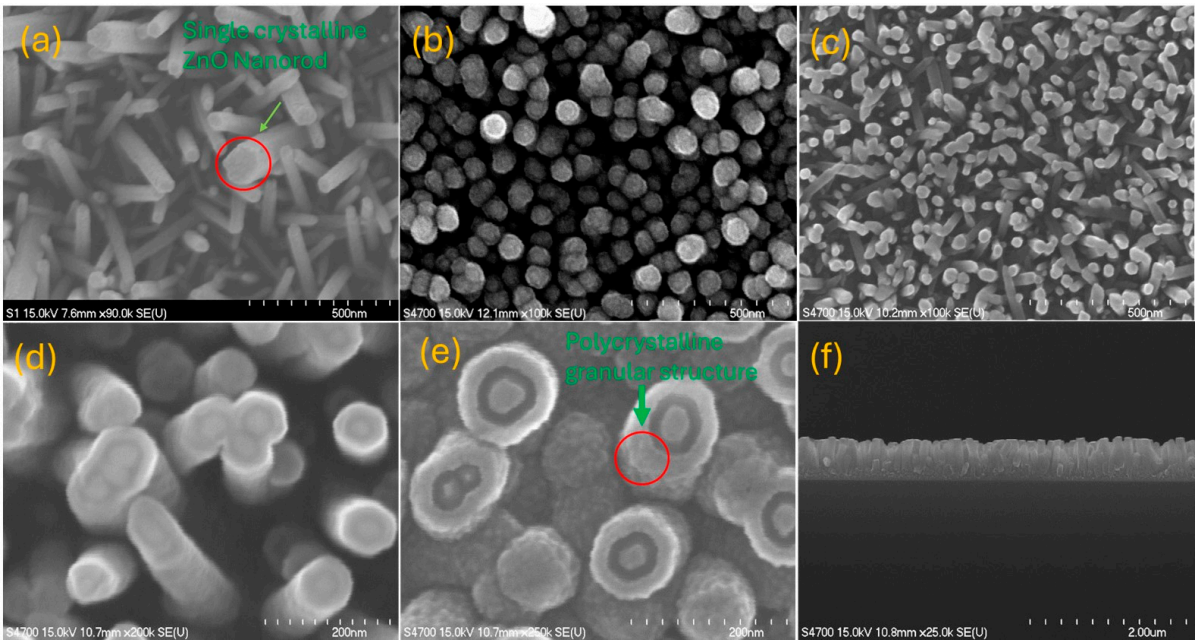

Figure 6. FE-SEM images of the novel nested ZnO thin-film nanorod/nanotube coaxial structure synthesis process. (**a**) Intrinsic hydrothermal ZnO nanorods with single-crystal hexagonal wurtzite structure. (**b**) Polycrystalline wrap-around ALD coating on ZnO nanorods after coating with an Al_2O_3 sacrificial film followed by ZnO thin films. (**c**,**d**) Reveals top cover removed by PIPS ion milling to expose the sacrificial layer. (**e**) Finally, the sacrificial layer has been preferentially etched away by a pH 11 NaOH solution. (**f**) Cross-section revealing an average nanorod height of ~750 nm.

For further physical characterization of the ALD-synthesized ZnO sensing films, we have conducted X-ray diffraction (XRD) analysis, energy-dispersive X-ray spectroscopy (EDS) and transmission electron microscopy (TEM). Figure 7a,b provides X-ray diffraction (XRD) results showing that ZnO films synthesized by ALD technology are polycrystalline with a preferred growth along the (002) plane or c-axis of the hexagonal wurtzite structure. Figure 7b demonstrates the progressive improvement of the full width at half maximum (FWHM), with increasing film thickness indicated by the number of ALD growth cycles. To investigate potential sample contamination, we ran energy-dispersive X-ray spectroscopy (EDS) for elemental chemical analysis using a scanning electron microscope (SEM) for our ALD ZnO film on Si substrate. The EDS of Figure 8 demonstrates that only Zn, O and Si signals were obtained, with no other detectable contaminants. This confirms the well-documented fact that atomic layer deposition (ALD) technology always provides undoped intrinsic semiconducting ZnO films without any detectable contamination based on the semiconductor-grade ALD precursors used to synthesize the ZnO films. The transmission electron microscopy (TEM) analysis corroborates the random polycrystalline nature of our ALD ZnO nanotubes. Figure 9a shows TEM micrographs of several detached ALD ZnO nanotubes harvested for TEM investigation. The grain structure of the polycrystalline ZnO nanotube walls can be clearly seen. Figure 9b zooms in for a high-resolution HR-TEM section of a ZnO nanotube wall to provide a detailed view of individual ZnO grains and the accompanying grain boundaries. The TEM micrographs provide a good summary of the physical properties of our ALD-synthesized nested nanotube films used for ethanol vapor sensing.

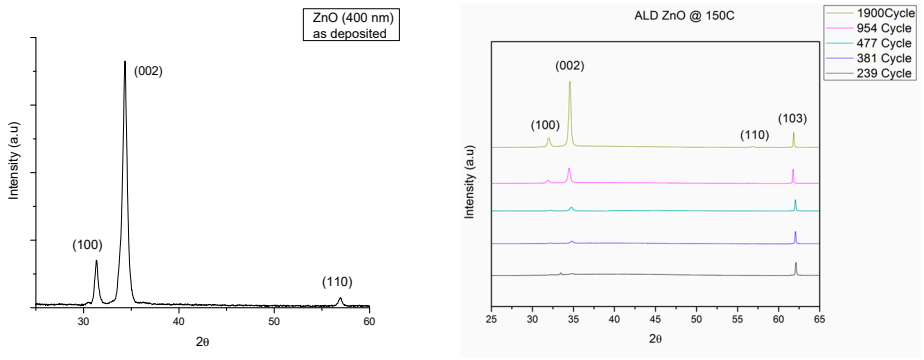

(**a**) (**b**)

Figure 7. (**a**) X-ray diffraction (XRD) results of a 400 nm ALD ZnO film synthesized by ALD technology, which results in a significant increase of the (002) peak, establishing preferred growth along the c-axis orientation of the hexagonal wurtzite structure. (**b**) XRD 2 θ scans as a function of the number of ALD growth cycles of ZnO, demonstrating that the ZnO film quality and the full width at half maximum (FWHM) are improving with increasing ALD ZnO film thickness.

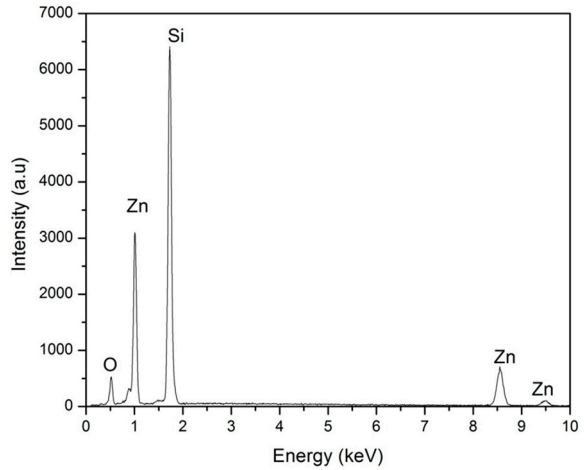

Figure 8. Energy-dispersive X-ray spectroscopy (EDS) for elemental chemical analysis of ALD ZnO film on Si substrate showing only Zn, O and Si signals, with no other detectable contaminants.

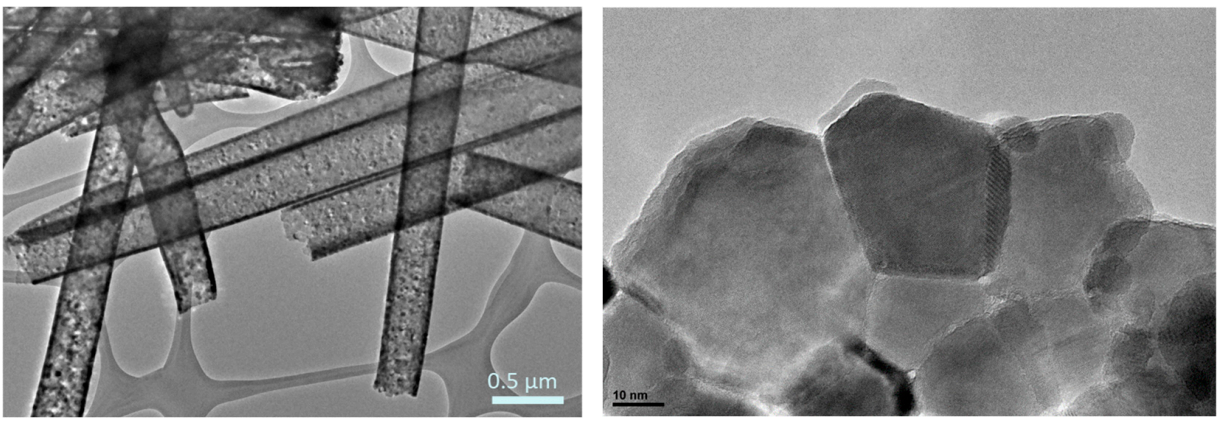

(**a**) (**b**)

Figure 9. (**a**) Transmission electron microscopy (TEM) of detached ALD ZnO nanotubes revealing the polycrystalline structure of the sensing film. (**b**) High-resolution HR-TEM micrograph providing details of the individual grains and grain boundaries of an ALD ZnO nanotube wall.

3.2. Sensing Response Analysis as a Function of Temperature

The sensing response was calculated based on the resistance change of the ZnO nanorod gas sensor relative to the concentration of ethanol vapor, as shown in Equation (4) [14]. Figure 10 shows the (a) resistance change and (b) response change of our novel ZnO nanostructure gas sensor initially after exposure to ethanol target vapor in the test tube at saturation level and optimum operating temperature of 320 °C, which was followed in the next step by completely exhausting the ethanol from the test set as shown in Figure 8.

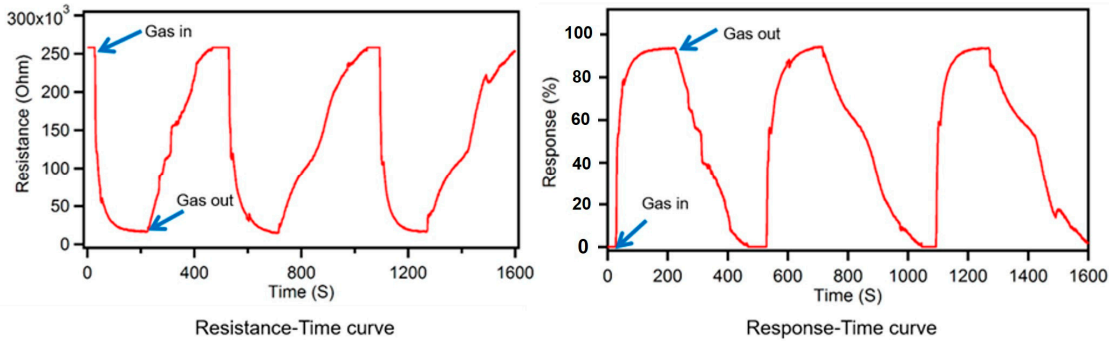

(**a**) (**b**)

Figure 10. Plots of (**a**) resistance change and (**b**) response change as a function of time of nested thin-film ZnO nanostructure gas sensors, delineating the response after introducing and exhausting the ethanol target vapor in a sealed testing chamber.

At the onset, our novel nested ZnO nanorod/nanotube gas sensors were tested at a constant saturation-level ethanol vapor concentration of 1000 ppm as a function of temperature from 25 °C to 340 °C. A sensing response comparison between our novel ZnO nanorod/nanotube gas sensor design and conventional ZnO nanorod gas sensors was performed, as shown in Figure 11. In both cases, the sensing response results of the novel nested ZnO thin-film nanorod/nanotube gas sensors compared to the conventional ZnO nanorod gas sensors demonstrate that the sensitivity response improves steadily with increasing temperature until a maximum value at 320 °C is reached, which constitutes the optimum working temperature, with more electrons generated at high temperature. After reaching the maximum peak at 320 °C, any further increase in temperature causes a decrease in sensitivity. This is attributed to the faster temperature-activated reaction ratio of the reduction reaction compared to the slower oxidation reaction ratio. At higher temperatures, there are more electrons adsorbed on the surface of ZnO from the conduction band, which causes an increase of the resistance and a decrease in the response change. Therefore, the sensing response of ZnO nanostructure gas sensors suffers a decrease at higher temperatures beyond the optimum working temperature.

Based on the comparison of the response versus temperature data shown in Figure 11, the novel nested ZnO thin-film nanorod/nanotube gas sensor design exhibits a higher sensing response compared to the conventional ZnO nanorod gas sensors. The advantage becomes more pronounced at lower temperatures, while the response difference between the two sensor designs narrows as the temperature approaches the optimum operating temperature. The observed enhancement in the sensing response is primarily attributed to the increased surface-to-volume ratio which was experimentally realized by our novel nested nanotube sensor design. After removing the Al_2O_3 sacrificial layer, a novel ZnO nanorod sensor was synthesized with coaxial nanotube structure, where the resulting empty annular ring space generated two additional ZnO reaction surfaces. Therefore, the chemical dissolution and removal of the Al_2O_3 sacrificial layer uncovered more reaction surfaces for ethanol vapor sensing in the same-sized area, which in turn resulted in a sizeable increase of the surface-to-volume ratio.

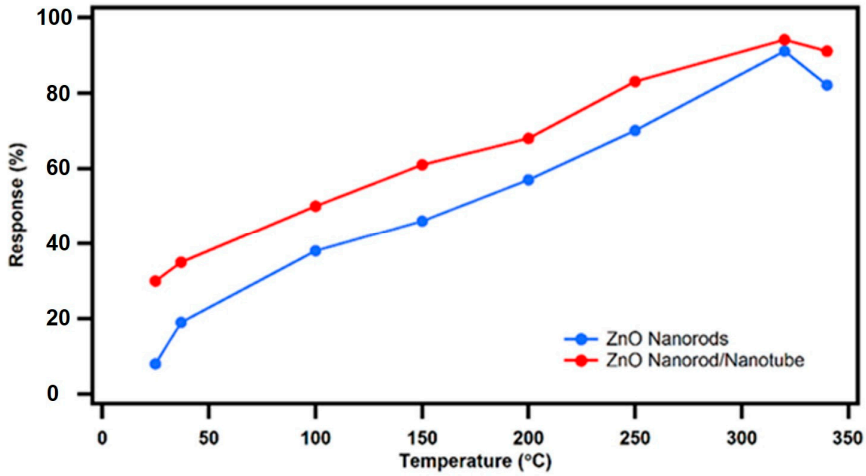

Figure 11. Sensing response result comparison between the novel nested ZnO thin-film nanorod/nanotube gas sensors with sacrificial annular gap (red curve) and the conventional ZnO nanorod gas sensors (blue curve) sensing response to saturation-level ethanol vapor concentration as a function of operating temperature.

3.3. Sensing Response Analysis as a Function of Various Ethanol Vapor Concentrations

Subsequently, the novel ZnO nanorod/nanotube gas sensors versus conventional ZnO nanorod gas sensors were tested as a function of various ethanol vapor concentrations ranging from 200 ppm to 1000 ppm at the confirmed optimum working temperature of 320 °C. The sensing response comparison between our nested ZnO nanorod/nanotube gas sensors versus conventional ZnO nanorod gas sensors is shown in Figure 12. Both sensing responses increase with increasing ethanol vapor concentration until they reach their saturation level. However, our nested ZnO thin-film nanorod/nanotube gas sensor design has achieved a higher sensing response compared to the conventional ZnO nanorod gas sensors from the comparison benchmark. It is especially noteworthy that the saturation level of our nested ZnO nanorod/nanotube gas sensor (1000 ppm) is higher than the level of the conventional ZnO nanorod gas sensor (800 ppm). The increased saturation level for the nested coaxial nanorod-in-nanotube approach is attributed to the available increased reaction surface from the ZnO nanotube. As a result, the saturation level of ZnO nanorod gas sensors is improved to 1000 ppm with nested coaxial ZnO nanotubes.

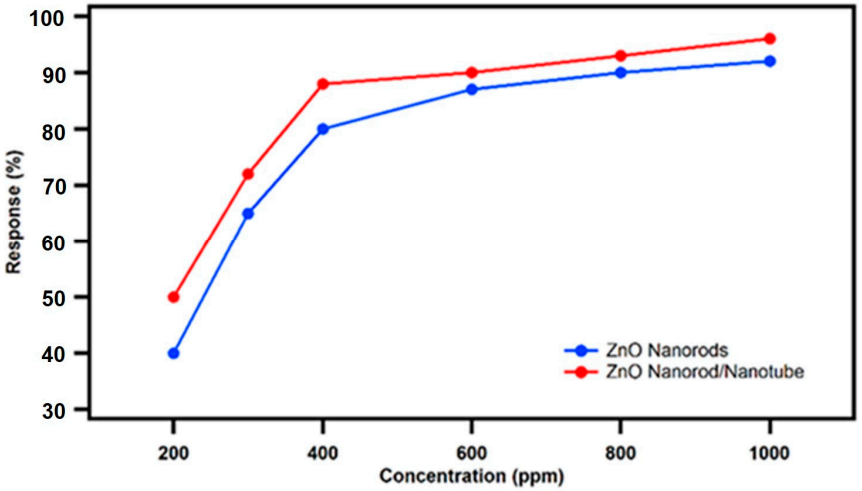

Figure 12. Sensing response comparison between the novel nested ZnO thin-film nanorod/nanotube gas sensors with sacrificial annular gap (red curve) and the conventional ZnO nanorod gas sensor (blue curve) sensing response as a function of different ethanol vapor concentrations at optimum operating temperature of 320 °C.

3.4. Gain in Sensing Response Enhancement

With increased surface-to-volume ratio, the sensing response of our novel nested ZnO nanorod/nanotube gas sensor design is improved compared to the original ZnO nanorod gas sensors. Figure 13 shows the additional enhancement gain of the novel nested ZnO nanorod/nanotube gas sensor when the sensor was operated under saturation-level concentration of ethanol target vapor at different temperatures. The maximum enhancement gain reached approximately 150% at 25 °C. The calculation formula is shown in Equation (6).

$$Gained\ Enhancement = \frac{R_{ZnO\ nested} - R_{ZnO\ nanorods}}{R_{ZnO\ nanorods}} \times 100\% \quad (6)$$

where $R_{ZnO\ nested}$ is the sensing response of the nested ZnO nanorod/nanotube gas sensors at saturation-level concentration of ethanol vapor, while $R_{ZnO\ nanorods}$ is the sensing response of the original ZnO nanorod gas sensors at saturation-level concentration of ethanol vapor at the same temperature.

$$Gained\ Enhancement\ at\ 25\ ^{\circ}C = \frac{0.32 - 0.126}{0.126} \times 100\% \approx 154\%$$

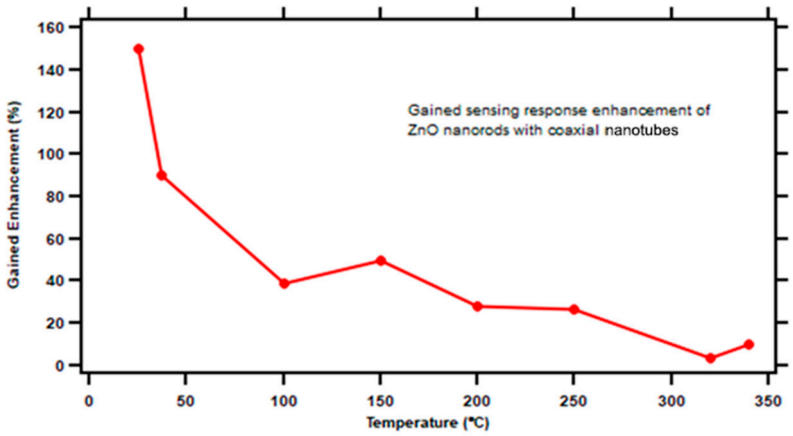

Figure 13. Gained sensing response enhancement of ZnO nanorod with nested coaxial nanotubes as a function of operating temperature.

3.5. The Relationship Between Surface-to-Volume Ratio and Sensitivity

During the gas detection step upon exposure to a reducing target gas, a reduction reaction occurs on the surface of ZnO gas sensors. Hereby, the following sensing reaction takes place between oxygen negative ions pre-existing on the sensor surface from the set operation and the reducing target gas molecules, as shown in Equation (7) [15].

$$X + O^{\delta-} \leftrightarrow X' + \delta e^{-} \quad (7)$$

where X is the target reducing gas, X' is the byproduct after the reaction and δ is the number of electrons.

Based on Equation (7), the electron density adsorbed to the surface can be calculated by Equation (8) [16].

$$n = \Gamma_t k_{gas} [O]^b [X]^b + n_0 \quad (8)$$

where n is the electron density under the target gas atmosphere, Γ_t is a time constant, n_0 is the electron density under the air atmosphere, b is a variable value (equal to 1 for O^- and 0.5 for O^{2-}), [O] is the adsorbed oxygen ion density, $[X]$ is the target gas molecule density

and k_{gas} is the reaction rate constant [13]. Therefore, based on Equation (4), the sensitivity relation is shown in Equation (9).

$$S_g = \left(\frac{R_{air} - R_{gas}}{R_{gas}}\right) = \frac{n_0 - n}{n_0} = \frac{n_0 - \left(\Gamma_t k_{gas}[O]^b[X]^b + n_0\right)}{n_0} = \frac{\Gamma_t k_{gas}[O]^b[X]^b}{n_0} \quad (9)$$

where S_g is the sensing response of the gas sensor. Conventionally, the surface-to-volume ratio can be defined by the adsorbed oxygen ion density [13]. Therefore, the adsorbed oxygen ion density can be defined by Equation (10).

$$[O] = \frac{\sigma_0 \varphi V_m}{V_S} \quad (10)$$

where σ_0 is the number of oxygen ions per unit area, V_m is the volume of the gas-sensitive material, φ is the ratio of surface area per volume of material (V_m) and V_S is the volume of the reaction chamber of the gas testing system [13]. After substituting Equation (10) into Equation (9), we can obtain the sensitivity of the gas sensor related to the surface-to-volume ratio from Equation (11).

$$S_g = \frac{\Gamma_t k_{gas}\left[\frac{\sigma_0 \varphi V_m}{V_S}\right]^b [X]^b}{n_0} \quad (11)$$

Equation (11) clearly explains the relationship between the sensitivity and the surface-to-volume ratio of MOS solid-state gas sensors. These equations provide much of the motivation background for this work and the concept of the novel nested ZnO thin-film sensor design architecture. With increased surface-to-volume ratio (σ_0 and φ) introduced by additional layers coating the coaxial ZnO nanotube, among them the sacrificial Al_2O_3 layer, the sensitivity of ZnO gas sensors to the ethanol vapor concentration detection correspondingly increases, based on Equation (11). Consequently, the sensitivity of ZnO nanorod gas sensors can be improved with an increased surface-to-volume ratio, which in our case is being realized by coaxial ZnO nanotubes, which expose two additional reaction surfaces after removal of the sacrificial alumina layer. Compared to the benchmarked experimental ZnO nanorods sample, the additional nanotube increased the reaction areas by about 150%. Approximately 70% of all nested nanotube structures were successfully opened up with the removal of the sacrificial layer. Therefore, after substituting $1.5\sigma_0$ and 1.5φ into the formula, there would be around 100% enhancement in the sensitivity, which is in agreement with the experiment result. Figure 6e reveals some wrap-around nested nanotubes that did not expose the sacrificial layer, because they did not reach the average height of 750 nm and consequently their top ALD capping layers were not cleared by the PIPS ion milling. Based on the FE-SEM analysis, about 70% of the nested nanorods were exposed by successful removal of the sacrificial Al_3O_2 layer. For the other 30%, the remaining surface cap stood in the way. It is worth noting that the ALD wrap-around coating worked on 100% of all nanorods. However, on 30% of the nested nanotube structures, the ALD surface capping layer was not removed, due to insufficient rod height.

It is also apparent that the process of ALD synthesis of wrap-around sacrificial films followed by ALD ZnO sensing film coatings can be continued to create even more complex nested ZnO thin-film nanostructures by adding additional nested films. Each new coaxial ALD ZnO film will further improve the surface-to-volume ratio and the device sensitivity. Depending on the application requirements, the device sensitivity can be increased to the desired sensitivity by adding n-numbers of additional free-standing coaxial ZnO films.

4. Conclusions

A novel nested coaxial ZnO thin-film nanorod/nanotube gas sensor architecture was fabricated by an integrated process combining hydrothermal growth of single-crystal nanorod center anchors, followed by 3D wrap-around coatings of sacrificial ALD alumina films alternating with ALD ZnO polycrystalline films. This novel nested ZnO thin-film gas

sensor architecture was examined by a newly upgraded gas sensor testing system connected with digital mass flow controllers for precise target vapor concentration. At the start, ZnO nanorods were synthesized by the hydrothermal method on a fine-grain polycrystalline ZnO seed layer deposited by ALD to anchor the final complex nested sensor nanostructure. An ALD Al_2O_3 sacrificial layer was a key concept to create nested coaxial ZnO thin-film nanotubes. After removing accumulated ALD films from the top surface by PIPS, the Al_2O_3 sacrificial layer was preferentially removed by wet chemical etching in a NaOH solution with pH 11. Consequently, a nested ZnO nanorod/nanotube structure was created with two additional reaction surfaces, which provide a significant increase in surface-to-volume ratio. In principle, our approach is amenable to adding more than one sacrificial layer and additional ZnO sensing films. Theoretically, every additional annular sacrificial layer will add two new ZnO reaction surfaces available for sensing after wet chemical etch removal. With increasing reaction surfaces and sites, the sensing response of nested ZnO thin-film nanorod gas sensors achieved a significant response enhancement, employing nested coaxial ZnO nanotubes with empty annular sacrificial layers. In particular, the saturation level was improved from 800 ppm to 1000 ppm. Compared to conventional ZnO nanorod gas sensor benchmarks, our novel nested ZnO nanotube gas sensors achieved a sensing response improvement of roughly 150% at a low temperature of 25 °C. In summary, this work demonstrates that our nanotechnology process design of creating empty annular gaps surrounding free-standing nested ZnO nanotubes is effective in increasing the surface-to-volume ratio and significantly improves the sensing response of ZnO solid-state gas sensors. Since the hydrothermal growth direction of the ZnO nanorods did not result in all nanorods aligned vertically along the [001] direction, PIPS could only remove the top cover of the highest nanorods, missing the inclined rods falling short on height. The formation ratio of successfully opened nested nanotube structures was around 70%, while 30% of the nanorods failed to have the ALD capping layer removed by ion milling because they did not reach the required rod height of 750 nm. In the future, the growth method will be optimized to achieve all vertically aligned ZnO nanorods, in which case the formation ratio will be improved to 100%. In addition, production reliability and repeatability will be optimized in the future for commercialization. This study is focused on the investigation of nested ZnO nanotube sensor designs based on DC resistance measurements with ohmic contacts to the ZnO samples. In general, this nested nanotube technology with sacrificial layers represents a pathway for further improvement of the sensitivity response and a higher saturation level, thereby enhancing the application potential of ZnO gas sensors for volatile organic compounds.

Author Contributions: Data curation; Formal analysis; experimental Investigation; methodology; writing-original draft, P.L.; assisting experimental Investigation, L.S.Z.; conceptualization, investigation, data curation, formal analysis and writing-original draft, K.Z.; supervision, funding acquisition, project administration; resources; conceptualization, validation, writing & editing original draft, H.B. All authors have read and agreed to the published version of the manuscript.

Funding: This research received no external funding.

Institutional Review Board Statement: Not applicable.

Informed Consent Statement: Not applicable.

Data Availability Statement: The original contributions presented in the study are included in the article, further inquiries can be directed to the corresponding author/s.

Conflicts of Interest: The authors declare no conflict of interest.

References

1. Kang, Y.; Yu, F.; Zhang, L.; Wang, W.; Chen, L.; Li, Y. Review of ZnO-based nanomaterials in gas sensors. *Solid State Ion.* **2021**, *360*, 115544. [CrossRef]
2. Khan, M.W.A.; Shaalan, N.M.; Ahmed, F.; Sherwani, S.; Aljaafari, A.; Alsukaibi, A.K.D.; Alenezi, K.M.; Al-Motair, K. Gas Sensing Performance of Zinc Oxide Nanoparticles Fabricated via Ochradenus baccatus Leaf. *Chemosensors* **2024**, *12*, 28. [CrossRef]

3. Aleksanyan, M.; Sayunts, A.; Shahkhatuni, G.; Simonyan, Z.; Shahnazaryan, G.; Aroutiounian, V. Gas Sensor Based on ZnO Nanostructured Film for the Detection of Ethanol Vapor. *Chemosensors* **2022**, *10*, 245. [CrossRef]
4. Wang, L.; Kang, Y.; Liu, X.; Zhang, S.; Huang, W.; Wang, S. ZnO Nanorod Gas Sensor for Ethanol Detection. *Sens. Actuators B Chem.* **2012**, *162*, 237–243. [CrossRef]
5. Hsueh, T.J.; Chang, S.J.; Hsu, C.L.; Lin, Y.R.; Chen, I.C. Promotion of the Electrochemical Activity of a Bimetallic Platinum-Ruthenium Catalyst by Oxidation-Induced Segregation. *J. Electrochem. Soc.* **2008**, *155*, 152–155. [CrossRef]
6. Kim, H.; Pak, Y.; Jeong, Y.; Kim, W.; Kim, J.; Jung, G.Y. Amorphous Pd-assisted H_2 Detection of ZnO Nanorod Gas Sensor with Enhanced Sensitivity. *Sens. Actuators B* **2018**, *262*, 460–468. [CrossRef]
7. Kakati, N.; Jee, S.H.; Kim, S.H.; Lee, H.K.; Yoon, Y.S. Sensitivity Enhancement of ZnO Nanorod Gas Sensors with Surface Modification by an InSb Thin Film. *Jpn. J. Appl. Phys.* **2009**, *48*, 105002. [CrossRef]
8. Xu, M.; Li, Q.; Ma, Y.; Fan, H. Ni-doped ZnO Nanorods Gas Sensor: Enhanced Gas-sensing Properties, C and DC Electrical Behaviors. *Sens. Actuators B* **2014**, *199*, 403–409. [CrossRef]
9. Hjiri, M.; Algessair, S.; Dhahri, R.; Albargi, H.B.; Mansour, N.B.; Assadid, A.A.; Neri, G. Ammonia gas sensors based on undoped and Ca doped ZnO nanoparticles. *RSC Adv.* **2024**, *14*, 5001–5011. [CrossRef] [PubMed]
10. Gu, D.; Baumgart, H.; Abdel-Fattah, T.M.; Namkoong, G. Synthesis of Nested Coaxial Multiple-Walled Nanotubes by Atomic Layer Deposition. *ACS Nano* **2010**, *4*, 753–758. [CrossRef] [PubMed]
11. Lin, P.; Chen, X.; Zhang, K.; Baumgart, H. Improved Gas Sensing Performance of ALD AZO 3-D Coated ZnO Nanorods. *ECS J. Solid State Sci. Technol.* **2018**, *7*, 246–252. [CrossRef]
12. Lin, P. Enhanced Sensing Performance of Novel Nanostructured ZnO Gas Sensors in Ethanol Vapor Concentration Detection Applications. Ph.D. Dissertation, Department of Electrical and Computer Engineering, Old Dominion University, Norfolk, VA, USA, 2019.
13. Pratzler, S.; Knopf, D.; Ulbig, P.; Scholl, S. Preparation of Calibration Gas Mixtures for the Measurement of Breath Alcohol Concentration. *J. Breath Res.* **2010**, *4*, 036004. [CrossRef] [PubMed]
14. Prajapati, C.S.; Sahay, P.P. Alcohol-sensing Characteristics of Spray Deposited ZnO Nano-particle Thin Films. *Sens. Actuators B Chem.* **2011**, *160*, 1043. [CrossRef]
15. Choopun, S.; Hongsith, N.; Wongrat, E. *Metal-Oxide Nanowires for Gas Sensor, Nanowires-Recent Advances*; IntechOpen: London, UK, 2012; Chapter 1.
16. Hongsith, N.; Wongrat, E.; Kerdcharoen, T.; Choopun, S. Sensor Response Formula for Sensor Based on ZnO Nanostructures. *Sens. Actuators B Chem.* **2010**, *144*, 67–72. [CrossRef]